Acta Biomaterialia xxx (xxxx) xxx

Contents lists available at ScienceDirect

Acta Biomaterialia

journal homepage: www.elsevier.com/locate/actbio

Full length article

Methylglyoxal alters collagen fibril nanostiffness and surface potential

Manuel Rufin[a], Mathis Nalbach[a], Maja Rakuš[a], Magdalena Fuchs[a], Mathias Poik[b], Georg Schitter[b], Philipp J. Thurner[a], Orestis G. Andriotis[a,*]

[a] Institute of Lightweight Design and Structural Biomechanics, TU Wien, Gumpendorfer Strasse 7, A-1060 Vienna, Austria
[b] Automation and Control Institute (ACIN), TU Wien, Gusshausstrasse 27–29, A-1040 Vienna, Austria

ARTICLE INFO

Article history:
Received 7 May 2024
Revised 14 August 2024
Accepted 23 August 2024
Available online xxx

Keywords:
Collagen
Glycation
Advanced glycation end products
Methylglyoxal
Nanoindentation
Surface potential
Atomic force microscopy
Kelvin probe force microscopy

ABSTRACT

Collagen fibrils are fundamental to the mechanical strength and function of biological tissues. However, they are susceptible to changes from non-enzymatic glycation, resulting in the formation of advanced glycation end-products (AGEs) that are not reversible. AGEs accumulate with aging and disease and can adversely impact tissue mechanics and cell-ECM interactions. AGE-crosslinks have been related, on the one hand, to dysregulation of collagen fibril stiffness and damage and, on the other hand, to altered collagen net surface charge as well as impaired cell recognition sites. While prior studies using Kelvin probe force microscopy (KPFM) have shown the effect glycation has on collagen fibril surface potential (i.e., net charge), the combined effect on individual and isolated collagen fibril mechanics, hydration, and surface potential has not been documented. Here, we explore how methylglyoxal (MGO) treatment affects the mechanics and surface potential of individual and isolated collagen fibrils by utilizing atomic force microscopy (AFM) nanoindentation and KPFM. Our results reveal that MGO treatment significantly increases nanostiffness, alters surface potential, and modifies hydration characteristics at the collagen fibril level. These findings underscore the critical impact of AGEs on collagen fibril physicochemical properties, offering insights into pathophysiological mechanical and biochemical alterations with implications for cell mechanotransduction during aging and in diabetes.

Statement of significance

Collagen fibrils are susceptible to glycation, the irreversible reaction of amino acids with sugars. Glycation affects the mechanical properties and surface chemistry of collagen fibrils with adverse alterations in biological tissue mechanics and cell-ECM interactions. Current research on glycation, at the level of individual collagen fibrils, is sparse and has focused either on collagen fibril mechanics, with contradicting evidence, or surface potential. Here, we utilized a multimodal approach combining Kelvin probe force (KPFM) and atomic force microscopy (AFM) to examine how methylglyoxal glycation induces structural, mechanical, and surface potential changes on the same individual and isolated collagen fibrils. This approach helps inform structure-function relationships at the level of individual collagen fibrils.

© 2024 The Author(s). Published by Elsevier Ltd on behalf of Acta Materialia Inc.
This is an open access article under the CC BY license (http://creativecommons.org/licenses/by/4.0/)

1. Introduction

Collagens constitute about 25% of the total human proteome, making them the most ubiquitous proteins in the human body [1]. Abundant collagen in the extracellular matrix (ECM), on the one hand, contributes to the mechanical integrity and function of connective tissues [2,3], and, on the other hand, plays an important role in cellular mechanotransduction [4-6], with implications for health and disease.

The unique molecular structure of collagen is characterized by the tight packing of three polypeptide chains into a triple helix. Certain collagen molecules (e.g., type I, III, and V) self-assemble into larger heterotypic constructs, known as collagen fibrils, which are the primary functional units of connective tissues [7-9]. The multiscale hierarchical organization allows collagen fibrils to fulfill mechanical properties tailored to specific tissue functions and to provide micro- and nanoscopic mechanical feedback to cells [4]. The collagen fibril mechanical feedback to cells is achieved through

* Corresponding author at: Gumpendorfer Strasse 7, A-1060 Vienna, Austria.
E-mail address: oandriot@ilsb.tuwien.ac.at (O.G. Andriotis).

https://doi.org/10.1016/j.actbio.2024.08.039
1742-7061/© 2024 The Author(s). Published by Elsevier Ltd on behalf of Acta Materialia Inc. This is an open access article under the CC BY license (http://creativecommons.org/licenses/by/4.0/)

Please cite this article as: M. Rufin, M. Nalbach, M. Rakuš et al., Methylglyoxal alters collagen fibril nanostiffness and surface potential, Acta Biomaterialia, https://doi.org/10.1016/j.actbio.2024.08.039

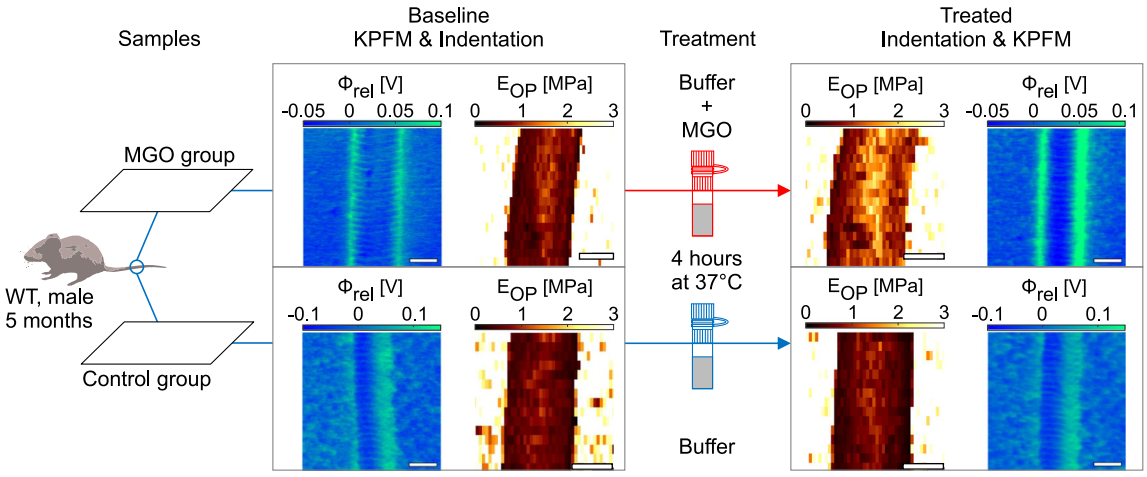

Fig. 1. Experimental workflow. Collagen fibrils from MGO and control groups were characterized with KPFM and AFM, before and after treatment with MGO + buffer (MGO group) or buffer only (Control group), respectively. Scale bars correspond to 300 nm.

cell attachments at specific loci on the surface of collagen fibrils [10].

Collagen fibrils are exposed to reducing sugars, which react with side groups of amino acids along the collagen triple helical structure; a process known as non-enzymatic glycation, leading to irreversible crosslink formation of advanced glycation end-products (AGEs) [11]. AGEs cross-links accumulate gradually with aging and disease, especially in diabetes [11]. Because AGEs are irreversible, they adversely affect tissue function and mechanical integrity, underscoring their significance in tissue aging and disease progression. For example, ribose crosslinking significantly reduced the post-yield tensile strain in tendons [12], but did not change their apparent elasticity. In the same study, Lee and Veres showed that ribose crosslinking hindered collagen fibrils from undergoing discrete plasticity in overloaded tendons [12]. Svensson et al. showed that methylglyoxal (MGO) crosslinking increased collagen fibril tensile strength, stiffness, and strain to failure [13].

Glycation, additionally affects collagen net charge [14] and molecular and cellular recognition [15,16] due to the reaction with charged lysine and arginine residues. By employing Kelvin Probe Force Microscopy (KPFM), Mesquida et al. showed a shift to more negative surface charge in glutaraldehyde-crosslinked collagen fibrils [17]. Bansode et al. showed evidence of collagen molecular reorganization within collagen fibrils as a result of ribose-5-phosphate glycation accompanied by altered surface charges [18]. Cells attach to the surface of collagen fibrils via metal ion-mediated interactions, and thus a surface charge shift may have implications for how cells attach, and ultimately how they sense and respond to changes of their microenvironment. In this context, MGO treatment has been reported to affect bacterial adhesion and biofilm formation, with implications to dental health [19,20].

Although there is an apparent influence of glycation on collagen fibril physicochemical properties, a gap in knowledge exists on how glycation-induced alterations in collagen fibril mechanics are linked to surface potential changes. Here, we utilized samples from a mouse tail-tendon, characterized by low initial cross-link density. We employed Kelvin Probe Force Microscopy (KPFM) to measure collagen fibril surface potential changes, and atomic force microscopy cantilever-based indentation to measure collagen fibril nanostiffness and hydration swelling changes on the same isolated and individual collagen fibrils before and after MGO treatment (Fig. 1). This multimodal KPFM/AFM approach allows us to isolate and examine the direct effects of MGO-induced cross-links on collagen fibril structure, mechanics, and chemical properties at the nanoscale. Through targeted MGO treatment, we simulated aging processes and diabetes-related changes observed in human tissues *in vivo*, providing a clearer understanding of the pathophysiological consequences of AGE accumulation at the collagen fibril level. Our approach shows the importance of characterizing both the nanoscale biochemical landscape and stiffness of collagen fibrils with implications in micro- and nanoscale assessment of native biological tissues and tissue models in health, aging, and disease.

2. Materials and methods

2.1. Sample preparation

Collagen fibrils were harvested from a 5-month-old male wild-type mouse tail-tendon fascicle (previously stored in −80 °C for several months before use). Samples were prepared on conventional lime glass microscope slides using a previously described method [21]. Briefly, the tail was skinned, and a section of tendon was dissected. The tendon was then kept hydrated in distilled water, and a single fiber was dissected and separated into two parts. Using sharp tweezers, each of the two fiber parts was opened and smeared out on a microscope slide. After a drying period of a few minutes, which enhances collagen fibril adhesion to the glass surface, the samples were thoroughly washed with distilled water and then stored in a vacuum desiccator. One glass slide was used for the MGO treatment and the other as a control group.

2.1.1. Individual and isolated collagen fibrils

Individual and isolated collagen fibrils ($N = 10$ per group) were identified from their characteristic 67 nm D-periodicity visible in atomic force microscopy (AFM) images recorded in air-dried conditions (Dimension Icon, Bruker; same as for Kelvin Probe Force Microscopy cf. Section 2.4.). We subsequently recorded optical microscope images for each position to identify the same collagen fibrils between various measurements (KPFM cf. §2.4 and nanomechanical cf. §2.3. tests conducted in different AFM setups). To further assure repeated measurements on the same regions of individual collagen fibrils, we chose our locations at a specific distance, typically a few micrometers, from characteristic fibril-fibril crossings.

2.2. MGO treatment

A buffer containing 20 mM MGO (Sigma Aldrich, St. Louis, MO, USA) and 5 mM EDTA in 10 mM phosphate buffered saline (PBS),

following the protocol of Svensson et al. [13] was used for the glycation of collagen fibrils. The buffer was adjusted to a pH 7.4 at 34 °C and stored in the fridge for a few days prior to the experiment. A negative control sample was treated in parallel with only the buffer. The microscope glass slides, with deposited collagen fibrils, were fully submerged in approximately 30 ml of the respective solution (buffer for negative control samples and buffer + MGO for glycation samples) in plastic tubes and stored in an incubator at 34 °C for 4 h. Subsequently, samples were thoroughly rinsed with distilled water for 1-2 min.

2.3. Nanomechanical characterization with AFM

2.3.1. AFM cantilever tip and spring constant calibration

An additional AFM (Nanowizard Ultraspeed A, Bruker JPK) was used, in force mapping mode, for nanoindentation tests. Nanoindentation measurements were performed in PBS (pH 7.4). To that end, 3D-printed rings were glued on the microscope slides with two-component dental silicon (picodent® twinduo extrahart). For all indentation experiments, we used the same rectangular PNP-DB-A cantilever (NanoWorld AG, Neuchâtel, Switzerland) with a nominal spring constant of 0.48 N/m (and measured at 0.11 N/m) and a nominal resonance frequency of 67 kHz. The geometry of the AFM tip was assessed by imaging a conical spike, with known tip radius and half-opening angle, from a TGT-1 calibration grating (ND-MDT Spectrum Instruments), as described previously [21]. The AFM tip geometry was reconstructed via a numerical deconvolution as described in [21,22].

The spring constant of the cantilever was calibrated in air via the thermal noise method, implemented in the JPK SPM Control software [23-26], prior to experiments in hydrated environment. After submerging the cantilever in PBS, we calibrated the inverse optical lever sensitivity, InvOLS, using a contact-based method [21] on the microscope glass slide surface, before each collagen fibril was mechanically assessed.

2.3.2. Force curve acquisition and nanostiffness estimation

Force maps were recorded on all 20 collagen fibrils, before and after MGO treatment, using a 1.5×1.5 µm² scan sized at 64×16 pixel resolution. One force map per collagen fibril was recorded for each measurement step in the workflow (Fig. 1).

The orientation of the force map was set such that the long axis of the collagen fibril was oriented along the 16-pixel axis (slow axis) and perpendicular to the 64-pixel axis (fast axis). Force curves were recorded at 1 nN relative setpoint (maximum applied force) and at 2 µm/s z-sensor extension speed. At 1 nN relative setpoint the resulting indentation depth did not exceed 10-15 % of the collagen fibril height, avoiding substrate effects [21].

The resulting force maps were then analyzed using a custom MATLAB program (https://github.com/Rufman91/ForceMapAnalysis). First, force curves underwent a base line and tilt correction by subtracting a line fit from a fraction of the non-contact domain of the approach curve. Then, the contact point was determined using a custom machine learning approach [27] and refined by a Hertz-Sneddon fit with a parabolic indenter model [28]. We then recovered the force vs. indentation data by correcting the raw force curves for the vertical tip deflection. The indentation modulus was estimated employing the Oliver-Pharr (OP) method [21,29,30] that assumes the unloading curve to result from linear elastic recovery based on the Hertzian contact theory [31]. The nanostiffness of collagen fibrils, expressed as the sample indentation modulus, E, was estimated via Eq. (1):

$$E = \sqrt{\pi}\frac{1-\nu}{2\beta}\frac{S_c}{\sqrt{A_c(h_c)}} \tag{1}$$

where S_c (N/m) is the contact stiffness, $A_C(h_c)(m^2)$, is the contact area, β is an empirical correction factor and was chosen as 1.0226 as a standard value given within the range suggested by Oliver and Pharr [29]. The correction factor β causes only a systematic error of max. 5% and does not influence any inter-cohort comparisons in this study. The Poisson's ratio ν was assumed to be 0.5 for an incompressible material [21,32-39], $h_c = h_{max} - \varepsilon P_{max}/S_c$ is the effective contact depth accounting for a sink-in at the non-contact surface, and with $\varepsilon = 0.73$ [29] (between a conical and paraboloid indenter) chosen according to the tip shape, which was determined by imaging a TGT1 calibration grating (NT-MDT Spectrum, Moscow, Russia) followed by a tip reconstruction algorithm [21].

For indentation modulus analysis, we included only data points from the apex of the collagen fibril, resulting in a total of 16 data points per collagen fibril per force map. Alongside the Oliver-Pharr method, we analyzed our indentation data with a classic Hertz-Sneddon fit with parabolic indenter model [28].

2.4. Kelvin Probe Force Microscopy (KPFM)

AFM dry height and KPFM surface potential imaging of air-dried collagen fibrils were performed on the Dimension Icon (Bruker) AFM. For KPFM measurements an Olympus AC-200TN-R3 (Olympus K.K., Shinjuku, Japan) cantilever with 9 N/m nominal spring constant and 150 kHz nominal resonance frequency (153.5 kHz measured frequency) was used. The conductive AFM chip was made of n-type silicon. Similarly to nanomechanical tests, the scan size was set to 1.5×1.5 µm² for each collagen fibril. In KPFM mode, the AFM operates in lift mode, i.e., the scan head passes over the same scan line twice. The first time, the sample height profile is measured in tapping mode, while on the second pass, the tip is scanned over the sample at a certain lift height with respect to the previously measured profile i.e., AFM head height. In our measurements, the lift height was set at 0 nm, meaning the distance to the surface was about half the setpoint amplitude of the tapping mode pass. We recorded 128 scan lines per image at 512 samples per line with a tip scan speed of 0.25 µm/s. Intermittent contact mode was driven at 153.34 kHz, i.e., just below the measured resonance peak, at a drive amplitude of roughly 1 V. Relative amplitude setpoint, drive amplitude, and I-gain were adjusted in between measurements to assure optimal imaging quality.

During the lift phase of a scan line, the surface potential was measured, by applying an alternating $U_{AC}(t)$ and a constant current U_{DC} to the cantilever tip. Here, the tip together with the conductive sample stage and the sample in between act as a capacitor setup where the force between the plates at given U_{AC}, U_{DC} and the local surface potential $\Phi(x,y)$ is given by:

$$F(t) = \frac{dC}{dz}V(t) \tag{2}$$

with

$$V(t) = U_{AC}\sin(\omega t) + (U_{DC} - \Phi(x,y)) \tag{3}$$

which results in a constant force F_{DC}, and time dependent forces at 2ω, $F_{2\omega}$, and ω, $F_\omega(t)$:

$$F_\omega(t) = \frac{dC}{dz}U_{AC}(U_{DC} - \Phi(x,y))\sin(\omega t) \tag{4}$$

The resulting cantilever deflection amplitude caused by the force component $F_\omega(t)$ is measured using a lock-in amplifier. Controlling $F_\omega(t)$ to be at zero by adjusting the constant current U_{DC} such that $(U_{DC} - \Phi(x,y)) = 0 = F_\omega(t)$, allows mapping of the surface potential directly by U_{DC}. Since, however, dC/dz is unknown, we cannot map the absolute surface potential (i.e. charges). Instead, we defined a relative surface potential for our collagen fibrils

that is given by the difference between the surface potential of the collagen fibril and the surface potential measured on the surrounding glass.

$$\Phi_{rel} = \Phi_{fib} - \Phi_{glass} \quad (5)$$

To this end, we extracted the potential and height image data from the raw data files into *.sdf* files using a custom PyGwy script in Gwyddion. The files were then loaded into our custom MATLAB program (https://github.com/Rufman91/ForceMapAnalysis). To avoid topological artifacts, occurring at the sides of the collagen fibrils, a stripe was automatically selected from the collagen fibril apex with a given fraction of the collagen fibril height as thickness for the surface potential of the collagen fibril Φ_{fib}. For Φ_{glass}, we chose the area surrounding the collagen fibril, manually excluding debris-contaminated locations. For each surface potential image, we calculated the relative collagen fibril surface potential as the difference of the means of both the chosen areas, i.e. $< \Phi_{fib} >$ and $< \Phi_{glass} >$.

2.5. Collagen fibril height and swelling ratio measurements

Collagen fibril dry height was measured in tapping mode (Dimension Icon, Bruker; cf. §2.4) and hydrated height was recorded in force volume map mode (Nanowizard Ultraspeed A, JPK-Bruker; cf. §2.3). Dry height profiles were recorded from the first pass of the KPFM measurements (cf. §2.4). The baseline was subtracted from 128 height profiles per collagen fibril, and the collagen fibril height was defined as the difference between the collagen fibril apex, and the baseline average height. The arithmetic mean of ca. 128 apex height values was taken as collagen fibril dry height H_{dry} (Fig. S1).

A height topography maps of hydrated collagen fibrils was extracted from each force volume map via the zero force contact point of each force-distance curves [27] (cf. §2.3.2). In total 16 profiles were recorded for every collagen fibril, the height was the difference between line profile baseline and collagen fibril apex, and an average collagen fibril hydrated height (H_{wet}) was calculated. The swelling ratio S_R of every collagen fibril was estimated as the fold-change in height by calculating the hydrated/dried height ratio, $S_R = H_{wet}/H_{dry}$. Additionally, we measured the collagen fibril cross-sectional area, and width in air-dried and hydrated samples, before and after treatment (MGO and buffer) (see Supporting Information). Morphological changes, attributed to random debris, were observed on AFM height topography in air-dried conditions. Such data were excluded from height data analysis. All collagen fibrils tested described had a hydrated height of at least 100 nm to avoid substrate effects during nanoindentation experiments.

2.6. Experimental workflow

Fig. 1 illustrates the experimental workflow. Two microscope slides with isolated collagen fibrils were prepared, as described above. We then let collagen fibrils hydrate for 2 hours in PBS (pH 7.4) and 5mM EDTA to recover from strains and stresses that might have occurred during the sample preparation. Samples were then subsequently rinsed with distilled water, air-dried, and stored in a low vacuum desiccator overnight. On the first measurement day, both slides were measured using the Kelvin Probe AFM setup. Here, 10 collagen fibrils were selected from each glass slide, and we measured their dry height and relative surface potential (baseline measurements, Fig. 1). Subsequently, 3D-printed ring-shaped fluid cells were attached to both glass slides using two-component dental silicon (picodent® twinduo extrahart). The fluid cell was filled with 5-6 ml of PBS (pH 7.4) and the setup was left to thermally equilibrate for 30 minutes. The hydrated collagen fibrils were assessed in force map mode for mechanical and height analysis (baseline measurements, Fig. 1). Both glass slides were subsequently submerged into their respective buffers, an MGO treatment buffer for the MGO group and a control buffer for the control group (as a negative control). After an incubation period of 4 hours at 34 °C, both slides were generously rinsed with distilled water, and fluid cells re-filled with PBS (pH 7.4) for further nanomechanical assessment (treated). Samples were then generously rinsed with distilled water and stored in the desiccator overnight. On the following day, KPFM measurements were performed on the same collagen fibrils after glycation.

2.7. Statistical analysis

Several metrics were analyzed comparing four groups against each other: control before vs. after treatment (only buffer) and MGO before vs. after treatment (Fig. 1). Each group contained 10 collagen fibrils, with the collagen fibrils being longitudinally paired between the before and after Control or MGO groups. To compare these groups, we assigned singular values to each collagen fibril for each metric.

For the indentation modulus, each collagen fibril had a maximum of 16 data points corresponding to individual force curves from the collagen fibril apex. Force curves showing slip-off events (Fig. S2) during indentation, were excluded from data analysis. The mean indentation modulus of the remaining force curves was then assigned to each collagen fibril. Similarly, the means of all data points of collagen fibril dry and hydrated height, and the relative surface potential were assigned to each individual collagen fibril. Basing the fibril properties on medians instead of means did not change the outcomes on all our subsequent statistical tests on the four groups. Due to measuring the same collagen fibrils before and after treatment, a paired statistical test was performed.

All groups passed the Kolmogorov-Smirnov test for normality tests. We then first assessed before vs. after treatment differences using paired t-tests, followed by tests for the difference of differences ($(\Delta E_{MGO} - \Delta E_{Control})$, $(\Delta \Phi_{MGO} - \Delta \Phi_{Control})$, $(\Delta D_{dry,MGO} - \Delta D_{dry,Control})$, $(\Delta D_{wet,MGO} - \Delta D_{wet,Control})$ and $(\Delta S_{R,MGO} - \Delta S_{R,Control})$ in Table S1) between the MGO and the control group using two-sample t-tests at a significance level of a=0.05. Testing the difference of differences between control and MGO group in every metric allows us to better control for unknown systematic errors between measurements.

3. Results

3.1. MGO treatment stiffens collagen fibrils

With a mean hydrated collagen fibril height of (191 ± 39) nm, the maximum indentation depths in the control ((12.4 ± 2.3) nm, $N = 30$) or glycated ((10.2 ± 1.6) nm, $N = 10$) group were well below the 10% threshold to avoid substrate effects [21,40,41]. Paired before-after t-tests reveal no significant changes in the control group, but a 2.33-fold increase in indentation modulus after MGO treatment. On average, the indentation modulus increased from (2.16 ± 0.73) MPa to (5.05 ± 1.74) MPa with MGO treatment (Fig. 1A, $p = 2.6e\text{-}5$). Hertzian analysis of the approach force-distance curves gave similar results (Fig. 2B, Fig. S3), i.e., equivalent statistical trends between groups. Additionally, both analysis models yield similar indentation moduli values (Fig. 2a, Fig. S3), i.e., no statistical difference was found in both control groups and the MGO group before treatment. This suggests elastic behavior of collagen fibrils in these groups. Interestingly, a paired t-test between the two analysis methods for the MGO group after treatment reveals significantly lower indentation moduli obtained with

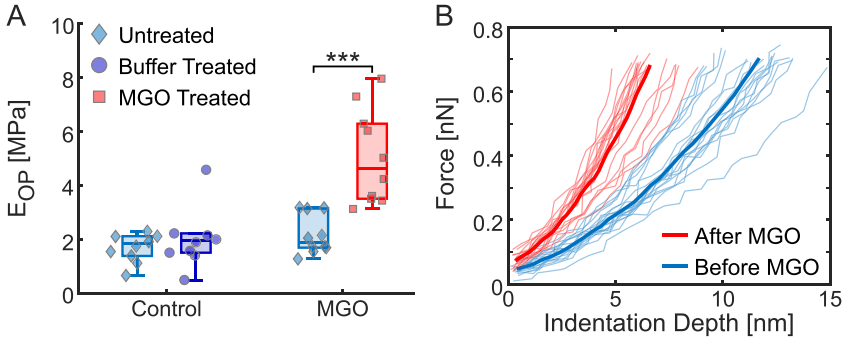

Fig. 2. MGO treatment led to a 2.3-fold increase in collagen fibril nanostiffness. (A) Indentation moduli (Oliver-Pharr method) of Control ($N = 9$) and MGO ($N = 10$) collagen fibrils, before and after treatment, i.e. with buffer only (Control) and MGO + buffer (MGO). (B) Individual (thin lines) and average (thick lines) force vs. indentation curves of an MGO-treated collagen fibril before (blue) and after (red) treatment. (***$p = 2.6e\text{-}5$).

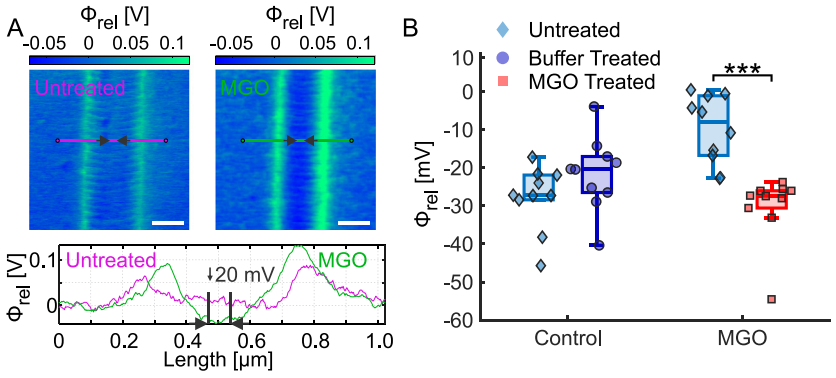

Fig. 3. MGO treatment decreased collagen fibril relative surface potential (Φ_{rel}). (A) Relative surface potential KPFM images and line profiles from an MGO-glycated collagen fibril before (magenta) and after (green) MGO treatment. In the line profile, an average drop of 20 mV was measured along the highlighted strip across the collagen fibril apex. (B) Relative surface potential data of Control and MGO groups (***$p = 2e\text{-}4$). Scale bars are 300 nm.

the Oliver-Pharr analysis (mean difference of 1.35 MPa, $p = 1.5e\text{-}5$). This may hint to a different material behavior (permanent, or viscoelastic and/or viscoplastic) of collagen fibrils after MGO treatment.

3.2. MGO treatment decreases collagen fibril surface potential

KPFM relative surface potential data were determined before and after treatment by subtracting the mean surface potential value from the surrounding glass (Fig. 3A) from a thin stripe from the collagen fibril apex (Fig. 3A line profiles). The stripe thickness was chosen such that the influence of edge effects is minimized. Both groups showed significant changes through treatment (buffer only or with MGO), albeit in opposite directions and to different effect sizes (Fig. 3A). The relative surface potential (Φ_{rel}) increased slightly from (-27.87 ± 8.4) mV to (-21.55 ± 9.67) mV in the control group, while in the MGO-treated group the Φ_{rel} showed a 3-fold decrease, from (-9.89 ± 8.99) mV to (-30.23 ± 8.94) mV.

3.3. MGO treatment changes collagen fibril height

MGO treatment affected both the air-dried and hydrated collagen fibril height and as a result, their swelling ratio upon hydration. Fig. 4A shows an exemplary image of the same collagen fibril in dry (KPFM first pass height %profiles) and hydrated state (in PBS, height topography from a force map) before and after MGO treatment. Corresponding profiles are displayed in Fig. 4C. Fig. 4 shows changes in collagen fibril height before and after treatment. On average, the height in MGO-treated collagen fibrils significantly increased in dry state from (108.7 ± 25.1) nm to (134.8 ± 26.4) nm ($p = 1.5e\text{-}6$, Fig. 4B), and in hydrated state (PBS), from (199.7 ± 34.7) nm to (209 ± 36.2) nm ($p = 0.003$, Fig. 4D). Notably, the effect size for the hydrated heights is rather small compared to the change in dry heights. Consequently, the swelling ratio was significantly decreased in MGO-glycated collagen fibrils from 1.86 ± 0.16 before to 1.56 ± 0.06 after treatment (***$p = 1e\text{-}4$, Fig. 4C and E). In agreement with height-based analysis, cross-sectional area (CSA) data show a statistically significant decrease in CSA swelling ratio for the MGO-treated group ($p = 0.043$, Fig. S5, panel E). We attribute the less prominent decrease in CSA swelling compared to height swelling ratio to the slightly smaller increase in collagen fibril dry CSA (Fig. S5, panel B).

4. Discussion

4.1. Nanoscale mechanics of MGO-treated collagen fibrils

Intrafibrillar cross-linking plays a major role in the mechanical properties of collagenous tissues. In the early tissue life cycle, such as during embryonic development, enzymatic crosslinks mediated by the lysyl oxidase family are formed to stabilize collagen fibril structure [42]. With maturation, the amount of enzymatic cross-links plateaus [43]. Yet, tissue stiffness at the fascicle level has been shown to further increase with glycation [13]. In association with diabetes, this effect is even stronger [44,45]. We show distinct changes in indentation modulus (i.e., nanostiffness), surface potential, and swelling behavior in individual collagen fibrils as a result of treatment with MGO.

MGO treatment led to increased indentation modulus in 10/10 hydrated collagen fibrils. At the collagen fibril level, Ahmed et al. [39] found a decrease in the indentation modulus of air-dried collagen fibrils within cryosections with increasing age, which they

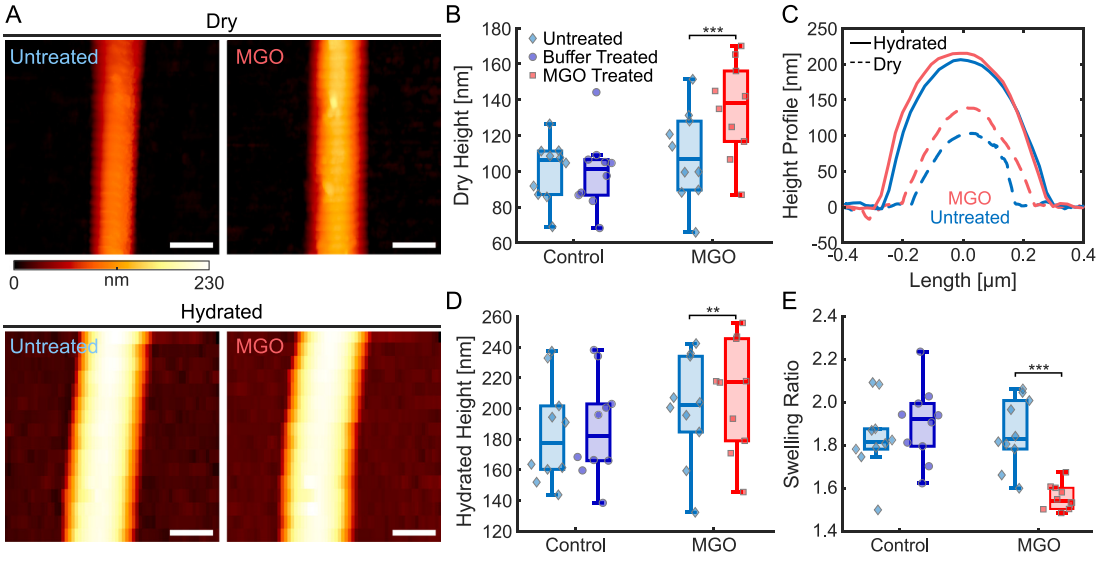

Fig. 4. MGO treatment alters hydration in collagen fibrils. (A) Height topography in air dry and hydrated of the untreated and MGO-treated collagen fibril. (B) Individual points represent the average dry height per collagen fibril in control and MGO groups. (C) Line profiles of the collagen fibril shown in panel A. (D) Average hydrated height per collagen fibril in control and MGO groups. (E) Average height swelling ratio is reduced (***p = 1e-4) in MGO-treated collagen fibrils. Scale bars are 300 nm. Collagen fibril size and swelling analysis based on cross-sectional area yielded similar results (Fig. S5).

connected to a higher amount of AGEs. This is in agreement with our results of increased collagen fibril dry height after MGO-treatment, which we interpret as increased amounts of residual water after air-drying and have shown in the past to play a role on dry collagen fibril indentation modulus [46]. Vaez et al. [47] performed indentation experiments on MGO-glycated collagen scaffolds and reconstituted collagen fibrils. In agreement with our data, they report increased indentation modulus of hydrated and MGO-glycated collagen scaffolds. In addition, Svensson et al. reported an increase of the tangent tensile modulus of collagen fibrils after MGO treatment [13]. At the fascicle level, Svensson et al. and Fessel et al. reported an increase in the tangent tensile modulus after 4.5h and 6h, respectively, of MGO treatment [13,48]. Contradictory to these findings, two earlier studies reported no significant effect on the tangent tensile modulus or stiffness of rat tail tendon fascicles after MGO treatment [49,50].

While there seem to be variable outcomes at the fascicle level, the only study investigating both, fibril and fascicle, scales [13] found an increase in tensile stiffness after MGO treatment on both levels. This is expected because collagen fibrils are the smallest reinforcing fibers of tendon tissue. Beyond the impact of collagen fibril stiffness on tissue-level mechanics, collagen fibrils compose the cellular microenvironment and contribute to the mechanical cues affecting and promoting cellular processes [51-53]. Hence, a biological response can be expected from increased collagen stiffness due to MGO treatment.

4.2. MGO treatment lowers the relative surface potential in isolated collagen fibrils

Nonenzymatic glycation in collagen is the reaction of reducing sugars, such as glucose, ribose, glyoxal, or methylglyoxal, with charged amino acids resulting in the formation of advanced glycation end products (AGEs) [54]. Lysine (Lys) and arginine (Arg) are targets of the most abundantly found AGEs such as Glucosepane, Pentosidine, GOLD, MOLD, MODIC, GODIC or DOGDIC [55-58]. Lys and Arg side groups are both positively charged at neutral pH. With their side chains being involved in forming electrically neutral AGEs through glycation, the overall surface potential of the collagen protein is expected to decrease toward more negative values [17]. In agreement with this hypothesis, our results show a reduction in relative surface potential in 10/10 fibrils after MGO treatment. Measuring tissue glycation via fluorescent AGEs (fAGEs) is an established and commonly used technique [59] but restricted to tissue level amounts of material. Using this technique on additional samples obtained from mouse tail-tendons treated with MGO vs. buffer did show a significant increase in fAGEs (Fig. S6 and S7). Surface potential measurements via KPFM allow for nanoscale qualitative changes due to glycation at the individual collagen fibril level. Relating surface potential data to individual collagen fibril mechanics helps tackle nanoscale heterogeneity. Our findings corroborate results from Mesquida et al., who showed a relative decrease in collagen fibril surface potential to treatment with glutaraldehyde [17] and ribose [18].

Importantly, the change in surface charge, measured via KPFM, may well have direct biological significance with implications in cell mechanotransduction. Cells interact with their microenvironment by using focal adhesions that connect the ECM components (collagen fibrils) with the cytoskeleton. By that, cells employ mechanisms that allow them to sense forces from the ECM and respond through mechanotransduction – cell function and behavior [60]. Glycation of Lys and Arg residues changes the length of their side chains and their charge distribution [61], while we expect this to affect the cellular integrin-binding-sites of collagen. On the one hand, changes in surface charge distribution may lead to altered molecular reorganization impeding the accessibility of integrin-binding sites. On the other hand, MGO and possibly other non-enzymatic reagents bind to Arg and effectively block binding motifs such as RGD, GER or GFO [62]. Such changes at the cell-ECM interface are expected to impact tissue homeostasis from altered cell-ECM interactions [16]. Glycation has been shown to have a deleterious effect on both integrin [63-66] and MMP [67] collagen binding sites, possibly impeding tissue degradation leading to dysregulation of physiological tissue remodeling processes. In addition to cell mechanotransduction, MGO treatment has also been reported to promote adhesion and biofilm formation of primary bacterial colonizers such as *Streptococcus mutans* [19,20].

While we reported a clear effect of MGO on collagen fibril mechanics and surface potential, there is no significant correlation between indentation modulus change and relative surface potential

within the MGO group (Fig. S4). This could be explained because KPFM does not differentiate between adducts and cross-links which influence nanostiffness or indentation modulus in opposite ways. Nevertheless, given the low numbers of collagen fibrils that can be assessed, approaches for chemical analysis at the individual collagen fibril level are highly important to further uncover correlations between mechanics and chemical modification.

4.3. MGO treatment affects collagen fibril (de-)hydration

Upon hydration with water, collagen fibrils increase in diameter compared to their air-dried state [38,68]. It is important to mention that the air-dried state is different from a fully dehydrated one, which is only achievable in low pressure environments and at high temperatures above 90 °C [69,70]. Water molecules interact with the collagen molecule in several distinct ways at varying degrees of affinity. Generally, water structurally binds readily to the polar sites at the collagen amino acid backbone by building single-molecule Ramachandran bridges or triple-molecule double bridges [69,70]. Only after most of the polar sites of the collagen molecule are covered in structurally bound water [68], secondary hydration occurs at the more hydrophobic surfaces. In our experiment, we measured altered hydration behavior in collagen fibrils after MGO treatment. Both dry and hydrated height increase significantly in 10/10 fibrils (Fig. 4B, D) after MGO treatment. The larger effect size in the dried compared to the hydrated state leads to a statistically significant decrease in apparent swelling after MGO treatment compared to non-glycated samples. At the molecular level, glycation has been associated with a two-fold effect on collagen fibril hydration. Firstly, newly formed AGE adducts were hypothesized to offer new sites for water hydration, leading to increased hydrated collagen fibril diameter [71]. Computational analysis validated this hypothesis, showed energetically favorable configurations of water molecules on multiple sites on the AGE cross-link glucosepane [39]. Secondly, cross-links may restrict shrinking upon air-drying, i.e., the space occupied by cross-links and amino acid side groups preventing the collagen backbones from getting closer to each other. These effects can explain the increase in air-dried collagen fibril height after glycation and the increase in hydrated height (Fig. 4B, C and D).

4.4. Limitations

In this study, collagen fibrils were harvested from a single animal and a single fascicle. While biological variation was not accounted for, our approach ensures consistency and control over experimental variables necessary to test the direct effect of glycation on the physicochemical properties of collagen fibrils.

Furthermore, we assessed the mechanical properties of collagen fibrils by utilizing AFM nanoindentation tests. In agreement with previous studies [21,32-39], we assumed the Poisson's ratio to be 0.5 (incompressible material). While the true Poisson's ratio of collagen fibrils is unknown, the assumption of 0.5 allows comparison to previous studies.

While AFM nanomechanical tests are highly informative and suitable for studying changes at the nanoscale [21,34,35,38,39] collagen fibrils are typically loaded in tension in most biological tissues. Additional studies incorporating tensile tests would therefore provide a more comprehensive understanding of glycation effects on collagen fibril mechanics. In this context, Svensson et al. (2018) reported increased initial stiffness and ultimate strength in MGO-glycated collagen fibrils under tension [13], which is in agreement with our findings.

The nature of AFM nanoindentation tests necessitates drying collagen fibrils on the substrate to achieve good adhesion. That means also during MGO treatment collagen fibrils are adhering to the substrate, potentially influencing the glycation process. While we cannot rule this potential effect out, our study design allows assessing the effect of MGO on the same fibril before and after treatment.

While methylglyoxal (MGO) is produced as a by-product of the Maillard reaction and is physiologically relevant to collagen fibril glycation, there are numerous other glycation agents (e.g., glucose, ribose, and glyoxal) that affect collagen fibril physicochemical properties. Compared to other glycation agents, MGO is characterized by a fast reaction, eliminating temporal effects such as pH reduction during glycation with ribose [72].

We conducted a fluorescent advanced glycation end products (fAGEs) assay to validate the formation of AGEs crosslinks. While we used different fascicles from a different animal for the fAGEs assay, our supplementary data (Fig. S6 and S7) clearly show the formation of AGEs through a glycation protocol, supporting the relevance of our findings.

The use of KPFM in our study was confined to dry state measurements. While this technique provided crucial insights into the changes in surface potential, future research could benefit from exploring these properties under hydrated conditions to better mimic the *in vivo* environment [73].

5. Conclusions

Here, we performed a multimodal KPFM/AFM approach to test the effect of methylglyoxal (MGO) treatment on the nanoscale mechanical and chemical properties of collagen fibrils. We found that MGO treatment; a) significantly increases nanostiffness (indentation modulus); b) decreases surface potential; and c) impacts the hydration of individual isolated collagen fibrils. Changes in nanostiffness and surface charge did not show significant correlations. Thus, further research is required to improve chemical analysis at the level of individual collagen fibrils for linking composition and chemical modifications to mechanical properties at this level. Our findings show how AGEs modify the structure and function of collagen fibrils, with implications for the development of age-related and diabetes-associated pathologies.

Ethics

All animal procedures were conducted in accordance with institutional and national guidelines. According to the Austrian animal experimentation law, permission from the Health Ministry was not required for this project since the harvesting of tissues or organs is not regarded as an animal experiment.

Funding

Manuel Rufin, Philipp J. Thurner and Orestis G. Andriotis acknowledge funding by the Vienna Science and Technology Fund (WWTF) [10.47379/LS19035].

Declaration of competing interests

The authors declare that they have no known competing financial interests or personal relationships that could have appeared to influence the work reported in this paper.

CRediT authorship contribution statement

Manuel Rufin: Writing – review & editing, Writing – original draft, Visualization, Validation, Software, Methodology, Investigation, Formal analysis, Data curation. **Mathis Nalbach:** Methodology, Investigation, Data curation. **Magdalena Fuchs:** Validation,

Methodology, Investigation, Formal analysis. **Mathias Poik:** Validation, Methodology, Investigation, Formal analysis. **Georg Schitter:** Writing – review & editing, Writing – original draft, Supervision, Resources, Project administration. **Philipp J. Thurner:** Writing – review & editing, Writing – original draft, Visualization, Supervision, Resources, Project administration, Funding acquisition, Conceptualization. **Orestis G. Andriotis:** Writing – review & editing, Writing – original draft, Visualization, Supervision, Resources, Project administration, Methodology, Funding acquisition, Conceptualization.

Acknowledgements

We gratefully acknowledge donation of murine tails by Prof. Peter Pietschmann from the Medical University of Vienna. The authors acknowledge TU Wien Bibliothek for financial support through its Open Access Funding Programme.

Supplementary materials

Supplementary material associated with this article can be found, in the online version, at doi:10.1016/j.actbio.2024.08.039.

References

[1] G.B. Smejkal, C. Fitzgerald, Revised estimate of total collagen in the human body, Int. J. Proteomics Bioinforma. 2 (1) (2017) 002–003 [Online]. Available: https://goo.gl/SFg4Dn .
[2] P. Fratzl, Collagen: structure and mechanics, an introduction, Collagen Struct. Mech. (2008) 1–13, doi:10.1007/978-0-387-73906-9_1.
[3] S.C. Cowin, S.B. Doty, Tissue mechanics, Tissue Mech. (2007) 1–682, doi:10.1007/978-0-387-49985-7/COVER.
[4] D. Dean, A.S. Nain, G.M. Genin, The mechanobiology of cells, fibers, and their interactions, Acta Biomater. 163 (2023) 1–6, doi:10.1016/j.actbio.2023.04.045.
[5] J. Jokinen et al., "Integrin-mediated cell adhesion to type I collagen fibrils*," 2004, 10.1074/jbc.M401409200.
[6] D. P. Mcdaniel et al., "The stiffness of collagen fibrils influences vascular smooth muscle cell phenotype," *Biophys. J.*, vol. 92, pp. 1759–1769, 10.1529/biophysj.106.089003.
[7] R.D.B. Fraser, T.P. MacRae, A. Miller, E. Suzuki, Molecular conformation and packing in collagen fibrils, J. Mol. Biol. 167 (2) (Jun. 1983) 497–521, doi:10.1016/S0022-2836(83)80347-7.
[8] D.J.S. Hulmes, T.J. Wess, D.J. Prockop, P. Fratzl, Radial packing, order, and disorder in collagen fibrils, Biophys. J. 68 (1995) 1661–1670, doi:10.1016/S0006-3495(95)80391-7.
[9] J.P.R.O. Orgel, A. Miller, T.C. Irving, R.F. Fischetti, A.P. Hammersley, T.J. Wess, The in situ supermolecular structure of type I collagen, Structure 9 (2001) 1061–1069.
[10] C. Cédric Zeltz, D. Gullberg, The integrin-collagen connection-a glue for tissue repair? J. Cell Sci. 129 (2016) 1284, doi:10.1242/jcs.188672.
[11] R.G. Paul, A.J. Bailey, Glycation of collagen: the basis of its central role in the late complications of ageing and diabetes, Int. J. Biochem. {\&} Cell Biol. 28 (12) (1996) 1297–1310, doi:10.1016/s1357-2725(96)00079-9.
[12] J.M. Lee, S.P. Veres, Advanced glycation end-product cross-linking inhibits biomechanical plasticity and characteristic failure morphology of native tendon, J. Appl. Physiol. 126 (4) (2019) 832–841, doi:10.1152/japplphysiol.00430.2018.
[13] R.B. Svensson, S.T. Smith, P.J. Moyer, S.P. Magnusson, Effects of maturation and advanced glycation on tensile mechanics of collagen fibrils from rat tail and Achilles tendons, Acta Biomater. 70 (Apr. 2018) 270–280, doi:10.1016/j.actbio.2018.02.005.
[14] S.A.C. Chong, et al., Methylglyoxal inhibits the binding step of collagen phagocytosis *, J. Biol. Chem. 282 (2007) 8510–8520, doi:10.1074/jbc.M609859200.
[15] I. Talior-Volodarsky, et al., Glycated collagen induces α11 integrin expression through TGF-β2 and Smad3, J. Cell. Physiol. 230 (2) (2015) 327–336, doi:10.1002/jcp.24708.
[16] A. Yuen, et al., Methylglyoxal-modified collagen promotes myofibroblast differentiation, Matrix Biol. 29 (6) (2010) 537–548, doi:10.1016/j.matbio.2010.04.004.
[17] P. Mesquida, et al., Evaluation of surface charge shift of collagen fibrils exposed to glutaraldehyde, Sci. Rep. 8 (1) (Jul. 2018), doi:10.1038/s41598-018-28293-1.
[18] S. Bansode, et al., Glycation changes molecular organization and charge distribution in type I collagen fibrils, Sci. Rep. 10 (1) (Feb. 2020) 3397, doi:10.1038/s41598-020-60250-9.
[19] C.M.A.P. Schuh, B. Benso, P.A. Naulin, N.P. Barrera, L. Bozec, S. Aguayo, Modulatory effect of glycated collagen on oral streptococcal nanoadhesion, J. Dent. Res. 100 (1) (Jan. 2021) 82–89, doi:10.1177/0022034520946320/SUPPL_FILE/DS_10.1177_0022034520946320.PDF.
[20] C. Leiva-Sabadini et al., "Nanoscale dynamics of streptococcal adhesion to AGE-modified collagen,", vol. 102, no. 8, pp. 957–964, May 2023, 10.1177/00220345231166294.
[21] O.G. Andriotis, et al., Nanomechanical assessment of human and murine collagen fibrils via atomic force microscopy cantilever-based nanoindentation, J. Mech. Behav. Biomed. Mater. 39 (Nov. 2014) 9–26, doi:10.1016/j.jmbbm.2014.06.015.
[22] D.J. Keller, F.S. Franke, Envelope reconstruction of probe microscope images, Surf. Sci. 294 (3) (Sep. 1993) 409–419, doi:10.1016/0039-6028(93)90126-5.
[23] J.E. Sader, J.W.M. Chon, P. Mulvaney, Calibration of rectangular atomic force microscope cantilevers, Rev. Sci. Instrum. 70 (10) (1999) 3967–3969, doi:10.1063/1.1150021.
[24] M.J. Higgins, et al., Noninvasive determination of optical lever sensitivity in atomic force microscopy, Rev. Sci. Instrum. 77 (1) (Jan. 2006) 1–5, doi:10.1063/1.2162455/349307.
[25] J.L. Hutter, J. Bechhoefer, Calibration of atomic-force microscope tips, Rev. Sci. Instrum. 64 (7) (1993) 1868–1873, doi:10.1063/1.1143970.
[26] H.J. Butt, M. Jaschke, Calculation of thermal noise in atomic force microscopy, Nanotechnology 6 (1) (Jan. 1995) 1, doi:10.1088/0957-4484/6/1/001.
[27] M. Rufin, M. Nalbach, P. J. Thurner, and O. G. Andriotis, "Using deep convolutional networks to find the contact point in nanoindentation force curves," *Prep.*
[28] I.N. Sneddon, The relation between load and penetration in the axisymmetric boussinesq problem for a punch of arbitrary profile, Int. J. Eng. Sci. 3 (1) (1965) 47–57, doi:10.1016/0020-7225(65)90019-4.
[29] W.C. Oliver, G.M. Pharr, An improved technique for determining hardness and elastic modulus using load and displacement sensing indentation experiments, J. Mater. Res. 7 (6) (Jun. 1992) 1564–1583, doi:10.1557/JMR.1992.1564.
[30] W.C. Oliver, G.M. Pharr, Measurement of hardness and elastic modulus by instrumented indentation: advances in understanding and refinements to methodology, J. Mater. Res. 19 (1) (Jan. 2004) 3–20, doi:10.1557/jmr.2004.19.1.3.
[31] H. Hertz, Über die Berührung fester elastischer Körper, J. Für Die Reine Angew. Math. 1882 (92) (1882) 156–171, doi:10.1515/crll.1882.92.156.
[32] O.G. Andriotis, et al., Structure–mechanics relationships of collagen fibrils in the osteogenesis imperfecta mouse model, J. R. Soc. Interface 12 (111) (Oct. 2015), doi:10.1098/RSIF.2015.0701.
[33] S.J. Baldwin, L. Kreplak, J.M. Lee, Characterization via atomic force microscopy of discrete plasticity in collagen fibrils from mechanically overloaded tendons: Nano-scale structural changes mimic rope failure, J. Mech. Behav. Biomed. Mater. 60 (2016) 356–366, doi:10.1016/j.jmbbm.2016.02.004.
[34] S. Baldwin, A. Quigley, C. Clegg, L. Kreplak, Nanomechanical mapping of hydrated rat tail tendon collagen I fibrils, Biophys. J. 107 (8) (2014) 1794–1801, doi:10.1016/j.bpj.2014.09.003.
[35] C.A. Grant, D.J. Brockwell, S.E. Radford, N.H. Thomson, Effects of hydration on the mechanical response of individual collagen fibrils, Appl. Phys. Lett. 92 (23) (Jun. 2008) 233902, doi:10.1063/1.2937001.
[36] C.A. Grant, D.J. Brockwell, S.E. Radford, N.H. Thomson, Tuning the elastic modulus of hydrated collagen fibrils, Biophys. J. 97 (11) (2009) 2985–2992, doi:10.1016/j.bpj.2009.09.010.
[37] C.A. Grant, M.A. Phillips, N.H. Thomson, Dynamic mechanical analysis of collagen fibrils at the nanoscale, J. Mech. Behav. Biomed. Mater. 5 (1) (Jan. 2012) 165–170, doi:10.1016/J.JMBBM.2011.08.020.
[38] A.J. Heim, W.G. Matthews, T.J. Koob, Determination of the elastic modulus of native collagen fibrils via radial indentation, Appl. Phys. Lett. 89 (18) (2006) 181902, doi:10.1063/1.2367660.
[39] T. Ahmed, et al., Combining nano-physical and computational investigations to understand the nature of 'aging' in dermal collagen, Int. J. Nanomedicine 12 (Apr. 2017) 3303–3314, doi:10.2147/IJN.S121400.
[40] M.P.E. Wenger, L. Bozec, M.A. Horton, P. Mesquida, Mechanical properties of collagen fibrils, Biophys. J. 93 (4) (Aug. 2007) 1255–1263, doi:10.1529/biophysj.106.103192.
[41] H. Bueckle, H. Westbrook, J. Conrad, The science of hardness testing and its research applications, Am. Soc. Met. (1973).
[42] J.E. Marturano, J.D. Arena, Z.A. Schiller, I. Georgakoudi, C.K. Kuo, Characterization of mechanical and biochemical properties of developing embryonic tendon, Proc. Natl. Acad. Sci. U. S. A. 110 (16) (Apr. 2013) 6370–6375, doi:10.1073/PNAS.1300135110/-/DCSUPPLEMENTAL.
[43] N.C. Avery, A.J. Bailey, Restraining cross-links responsible for the mechanical properties of collagen fibers: natural and artificial, Collagen Struct. Mech. (2008) 81–110, doi:10.1007/978-0-387-73906-9_4.
[44] T.T. Andreassen, K. Seyer-Hansen, A.J. Bailey, Thermal stability, mechanical properties and reducible cross-links of rat tail tendon in experimental diabetes, Biochim. Biophys. Acta - Gen. Subj. 677 (2) (Oct. 1981) 313–317, doi:10.1016/0304-4165(81)90101-X.
[45] S. L. Schnider and R. R. Kohn, "Effects of age and diabetes mellitus on the solubility of collagen from human skin, tracheal cartilage and dura mater," vol. 17, pp. 185–194, 1982.
[46] O.G. Andriotis, et al., Structure{\textendash}mechanics relationships of collagen fibrils in the osteogenesis imperfecta mouse model, J. R. Soc. Interface 12 (111) (2015) 20150701, doi:10.1098/rsif.2015.0701.
[47] M. Vaez, et al., Modulation of the biophysical and biochemical properties of collagen by glycation for tissue engineering applications, Acta Biomater 155 (2023) 182–198, doi:10.1016/j.actbio.2022.11.033.

[48] G. Fessel, et al., Advanced glycation end-products reduce collagen molecular sliding to affect collagen fibril damage mechanisms but not stiffness, {PLoS} {ONE} 9 (11) (Nov. 2014) e110948, doi:10.1371/journal.pone.0110948.
[49] Y. Li, G. Fessel, M. Georgiadis, J.G. Snedeker, Advanced glycation end-products diminish tendon collagen fiber sliding, Matrix Biol 32 (3–4) (Apr. 2013) 169–177, doi:10.1016/J.MATBIO.2013.01.003.
[50] G. Fessel, J. Wernli, Y. Li, C. Gerber, J.G. Snedeker, Exogenous collagen cross-linking recovers tendon functional integrity in an experimental model of partial tear, J. Orthop. Res. 30 (6) (Jun. 2012) 973–981, doi:10.1002/jor.22014.
[51] O. Chaudhuri, J. Cooper-White, P.A. Janmey, D.J. Mooney, V.B. Shenoy, Effects of extracellular matrix viscoelasticity on cellular behaviour, Nature 584 (2020) 535, doi:10.1038/s41586-020-2612-2.
[52] C.T. Mierke, Viscoelasticity, like forces, plays a role in mechanotransduction, Front. Cell Dev. Biol. 10 (2022) 1–58 no. February, doi:10.3389/fcell.2022.789841.
[53] K.M. Yamada, A.D. Doyle, J. Lu, Cell–3D matrix interactions: recent advances and opportunities, Trends Cell Biol 32 (10) (2022) 883–895, doi:10.1016/j.tcb.2022.03.002.
[54] J.G. Snedeker, A. Gautieri, The role of collagen crosslinks in ageing and diabetes - the good, the bad, and the ugly, Muscles. Ligaments Tendons J. 4 (3) (Jul. 2014) 303–308 [Online]. Available: http://www.ncbi.nlm.nih.gov/pubmed/25489547 .
[55] D.R. Sell, K.M. Biemel, O. Reihl, M.O. Lederer, C.M. Strauch, V.M. Monnier, Glucosepane is a major protein cross-link of the senescent human extracellular matrix: relationship with diabetes *, J. Biol. Chem. 280 (13) (Apr. 2005) 12310–12315, doi:10.1074/JBC.M500733200.
[56] D.R. Sell, V.M. Monnier, Structure elucidation of a senescence cross-link from human extracellular matrix: implication of pentose in the aging process, J. Biol. Chem. 264 (36) (1989) 21597–21602, doi:10.1016/S0021-9258(20)88225-8.
[57] R.H. Nagaraj, I.N. Shipanova, F.M. Faust, Protein cross-linking by the Maillard reaction. Isolation, characterization, and in vivo detection of a lysine-lysine cross-link derived from methylglyoxal, J. Biol. Chem. 271 (32) (Jan. 1996) 19338–19345, doi:10.1074/jbc.271.32.19338.
[58] M. O. Lederer and R. G. Klaiber, “Cross-linking of proteins by maillard processes: characterization and detection of Lysine±Arginine cross-links derived from glyoxal and methylglyoxal.”
[59] D.R. Sell, V.M. Monnier, Isolation, purification and partial characterization of novel fluorophores from aging human insoluble collagen-rich tissue, Connect. Tissue Res. 19 (1) (1989) 77–92, doi:10.3109/03008208909016816.
[60] M.A. Schwartz, D.W. DeSimone, Cell adhesion receptors in mechanotransduction, Curr. Opin. Cell Biol. 20 (5) (Oct. 2008) 551–556, doi:10.1016/J.CEB.2008.05.005.
[61] R. Li, et al., In situ characterization of advanced glycation end products (AGEs) in collagen and model extracellular matrix by solid state NMR, Chem. Commun. 53 (100) (Dec. 2017) 13316–13319, doi:10.1039/C7CC06624D.
[62] J. Emsley, C.G. Knight, R.W. Farndale, M.J. Barnes, R.C. Liddington, Structural basis of collagen recognition by integrin $\alpha 2\beta 1$, Cell 101 (1) (Mar. 2000) 47–56, doi:10.1016/S0092-8674(00)80622-4.
[63] R.G. Paul, A.J. Bailey, The effect of advanced glycation end-product formation upon cell-matrix interactions, Int. J. Biochem. Cell Biol. 31 (6) (Jun. 1999) 653–660, doi:10.1016/S1357-2725(99)00023-0.
[64] A.D. McCarthy, T. Uemura, S.B. Etcheverry, A.M. Cortizo, Advanced glycation endproducts interfere with integrin-mediated osteoblastic attachment to a type-I collagen matrix, Int. J. Biochem. Cell Biol. 36 (5) (May 2004) 840–848, doi:10.1016/J.BIOCEL.2003.09.006.
[65] A.J. Bailey, R.G. Paul, L. Knott, Mechanisms of maturation and ageing of collagen, Mech. Ageing Dev. 106 (1–2) (1998) 1–56, doi:10.1016/s0047-6374(98)00119-5.
[66] Y. Okano, H. Masaki, H. Sakurai, Dysfunction of dermal fibroblasts induced by advanced glycation end-products (AGEs) and the contribution of a nonspecific interaction with cell membrane and AGEs, J. Dermatol. Sci. 29 (3) (Sep. 2002) 171–180, doi:10.1016/S0923-1811(02)00021-X.
[67] J.D. Mott, R.G. Khalifah, H. Nagase, C.F. Shield, J.K. Hudson, B.G. Hudson, Nonenzymatic glycation of type IV collagen and matrix metalloproteinase susceptibility, Kidney Int. 52 (5) (Nov. 1997) 1302–1312, doi:10.1038/KI.1997.455.
[68] O.G. Andriotis, S. Desissaire, P.J. Thurner, Collagen fibrils: nature’s highly tunable nonlINEAR SPRings, ACS Nano 12 (4) (Apr. 2018) 3671–3680, doi:10.1021/acsnano.8b00837.
[69] G. D. Fullerton, M. Amurao, A. Rahal, and I. L. Cameron, “Micro-CT dilatometry measures of molecular collagen hydration using bovine extensor tendon; micro-CT dilatometry measures of molecular collagen hydration using bovine extensor tendon,” 2010, 10.1118/1.3514123.
[70] G. D. Fullerton and M. R. Amurao, “Evidence that collagen and tendon have monolayer water coverage in the native state,” 10.1016/j.cellbi.2005.09.008.
[71] O. G. Andriotis, K. Elsayad, D. E. Smart, M. Nalbach, D. E. Davies, and P. J. Thurner, “Hydration and nanomechanical changes in collagen fibrils bearing advanced glycation end-products,” 2019, 10.1364/BOE.10.001841.
[72] D. Vashishth, G.J. Gibson, J.I. Khoury, M.B. Schaffler, J. Kimura, D.P. Fyhrie, Influence of nonenzymatic glycation on biomechanical properties of cortical bone, Bone 28 (2) (Feb. 2001) 195–201, doi:10.1016/S8756-3282(00)00434-8.
[73] T. Hackl, G. Schitter, and P. Mesquida, “AC Kelvin probe force microscopy enables charge mapping in water,” 2022, 10.1021/acsnano.2c07121.